Parameter Estimation for Models of NH_4^+ Transport by the Renal Na-K-2Cl and K-Cl Cotransporters

Mariano Marcano,[1,*] Hun-Mo Yang,[2] Aniel Nieves-González,[3] Mónica Nadal-Quirós,[1] Chris Clausen,[4] and Leon C. Moore[4]

[1]*Department of Computer Science, University of Puerto Rico, Río Piedras, PR 00936-8377*
[2]*Department of Physiology, Soonchunhyang University, Chungnam, Republic of Korea*
[3]*Department of Applied Mathematics and Statistics, SUNY, Stony Brook, NY 11794-3600*
[4]*Department of Physiology and Biophysics, SUNY HSC, Stony Brook, NY 11794-8661*

February 22, 2011

Abstract

An optimization algorithm was used to compute parameter values for kinetic models of NH_4^+ transport by the renal Na-K-2Cl cotransporter (NKCC2) and K-Cl cotransporter (KCC). The optimization method finds model off-binding and translocation rate constants by minimizing the difference between model unidirectional fluxes and published data on NH_4^+-dependent $^{86}Rb^+$ uptake by the NKCC and KCC transporters in transfected *Xenopus* oocytes. The computed parameters for each model yielded fluxes consistent with the experimental curves. However, a systematic exploration of the parameter space revealed that, in some models, different parameter sets yield essentially identical fits to the data. With the identified parameters, the NKCC models show K^+/NH_4^+ exchange and enhancement of Na^+ uptake by NH_4^+ binding when external K^+ concentration is low. Further, under these conditions, substantial rates of K^+/NH_4^+ exchange are predicted, which may prevent depletion of luminal K^+. For the KCC models, in the medulla where the interstitial concentration of ammonium is high, substantial rates of K^+/NH_4^+ exchange are again predicted to occur.

Key words epithelial transport; thick ascending limb; kidney; nonlinear optimization

1 Introduction

A mathematical model of ion transport in an epithelial cell of the thick ascending limb (TAL) must include models of the renal Na-K-2Cl cotransporter (NKCC2) and the K-Cl cotransporter (KCC1 and KCC4), because they are important mechanisms for ion uptake across the cell membranes and they participate in the regulation of cytosolic Cl^-, which is important in lumen-to-serosa Na^+ transport and in the regulation of cell volume. These transporters also transport ammonium, which competes with K^+ for binding [9, 11, 20]. Thus, any TAL cell model must also include NKCC and KCC cotransporter models that allow Na-NH_4-2Cl and NH_4-Cl cotransport, respectively.

In this work, we use mathematical models to simulate the transport of Na^+, Cl^-, K^+, and NH_4^+ across a TAL cell by the NKCC and KCC with ammonium and potassium being able to compete with each other for a binding site in the transporter. Our models are based on the reaction sequence proposed by Lytle and McManus [12] and by Lytle et al. [13] for the NKCC. We assume a similar, but truncated, sequence for the KCC cotransporters because they all are members of the SLC cation-chloride cotransporter family, whose members share some common structures [10].

*Corresponding author. *E-mail address*: mariano.marcano@upr.edu (Mariano Marcano)

The models are illustrated in Figures 1 and 2. In each figure there are two cycles; the inner one represents the binding sequence of the KCC (Figure 1) and NKCC (Figure 2); the outer cycle represents the binding sequence when NH_4^+ substitutes for K^+. The presence of two linked cycles suggests that these transporters may also act as K^+/NH_4^+ exchangers, a transport mode that may be important in preventing the depletion of K^+ in the TAL lumen.
For a given parameter set (binding and translocation rate constants) and intra- and extracellular ligand concentrations, the solution of a cotransporter model yields the cotransporter distribution among the possible states in the assumed kinetic scheme. From this distribution, unidirectional and net ion fluxes can be determined. Furthermore, we computed model rate constants by solving optimization problems to fit the model unidirectional fluxes to experimental fluxes reported in the literature [3, 15, 17].
Benjamin and Johnson [2] formulated the system of differential equations that describes the kinetic reactions for the NKCC model. Moreover, they solved an optimization problem to obtain model rate constants by fitting the model unidirectional fluxes to a variety of experimental data for the NKCC.
In [14], by using a similar approach to the one of Benjamin and Johnson [2] and data from three variants of the NKCC2 isoform in the TAL, we computed rate constants that led to transport models that were more specific to the kidney. To compute such constants we solved optimization problems to fit the model fluxes to experimental values. However, the optimization problems exhibit multiple solutions in the sense that different sets of parameters yield similar fits. This causes a computational difficulty because optimization methods may compute a solution that is not the best optimum. To deal with such difficulty, in [14] we developed an algorithm that systematically explores the parameter space seeking optimal parameter solutions. Moreover, by testing different model assumptions with respect to symmetry of the rate constants, in [14] we did not find any significant difference between the model proposed by Benjamin and Johnson [2] and models that remove the symmetry assumptions. Hence, in the present work, we use the model assumptions proposed by Benjamin and Johnson [2] regarding rate constant symmetry (*vide infra*). Our models consist of systems of linear equations, whose numbers vary from five to fourteen. These linear systems are the steady-state equations of the dynamical systems derived from the kinetic models (see Figures 1 and 2), which consist of systems of ordinary differential equations.
Recently, Weinstein [21] formulated simplified models for NKCC and KCC with ammonium transport by assuming rapid equilibrium. By introducing this assumption, Weinstein could reduce the systems of linear equations to two linear equations which could be solved analytically to compute the unidirectional fluxes. The author used data reported in [15, 17] to obtain rate constants by fitting the NKCC and KCC models to the kinetic curves. Then physiological arguments were used to choose the NH_4^+ binding rate constant and the outer-cycle translocation rate for both models. To deal with the computational difficulty arising from multiple sets of parameters (*vide supra*), the author argued that, for the simplified models, there are some degrees of freedom in parameter choice. By using this and other physiological arguments, he fixed the values of some translocation rates, which reduced the dimension of the parameter space. Despite this, the existence of multiple solutions of optimal parameters was reported. Moreover, for the NKCC2A and NKCC2B he reported a fitting error of about 25%.
In the present work, we compute parameters for the model of the NKCC with NH_4^+ (Figure 2) by fitting the model unidirectional fluxes to the data reported in [3, 17]. Similarly, for the parameters of the model of the KCC with NH_4^+ (Figure 1) we use the data reported in [3, 15]. In that way, by solving optimization problems we are able to compute values for all the parameters in Figures 1 and 2. The resulting models fit the measured data well. In both transporters, the

competition between NH_4^+ and K^+ for binding is evident, and the presence of NH_4^+ can augment both Na^+ uptake by NKCC2 and Cl^- transport by the KCC transporter. Further, the models predict significant K^+/NH_4^+ exchange by the NKCC2 transporter when luminal Na^+, K^+ and Cl^- concentrations are low, and by the KCC transporter when interstitial NH_4^+ concentration is high.

2 Mathematical Model

The models are based on the models published in [2, 14], which in turn are based on the kinetic model proposed in [12, 13]. In the construction of the models we assume first-order binding kinetics and conservation of cotransporter, and impose parameter constraints to satisfy the laws of thermodynamics.

In the models we assume that the on-binding rate constant ($k$on) is the same for all ions and its value is 10^8 l·mol^{-1}·s^{-1} as others have done before [2, 5, 14]. This value is close to 6×10^8 l·mol^{-1}·s^{-1}, which is the value found by van Holde [19] for the rate constant of the binding of small ligands to specific sites on macromolecules. We further assume symmetrical binding, in that, for each ion, the off-binding rate constant in the external side of the cell is equal to the value in the intracellular side as has been assumed before [2, 21]. Further, for the NKCC model, we assume that the two Cl^- binding sites have the same off-binding rate, an assumption made in earlier models [2, 21]. We assume first-on first-off binding order (glide symmetry) as was done in [2, 13, 14, 21], and as suggested by experimental results by Gagnon et al. [7, 8]. In a previous model of the NKCC, Marcano et al. [14] evaluated four models with different symmetry assumptions, which included different off-binding rates for the Cl^- sites and different off-binding rates for K^+ in the luminal side of the cell and in the cytosolic side; comparison of the fits of the four resultant models to experimental data showed only small differences.

The differential equations that govern the models for the KCC and NKCC are shown in the Appendix. At steady-state, $\mathrm{d}E_j/\mathrm{d}t = 0$ for all j, and each model reduces to a system of linear equations, which can be written as

$$A\mathbf{e} = \mathbf{b}, \tag{1}$$

where $\mathbf{e}$ is the vector containing the fraction of cotransporters in each state (E_j). Both the matrix A and the vector $\mathbf{b}$ depend on the binding, release, and translocation rate constants.

Once the linear system is solved, the values of the fraction of cotransporter states E_j's are used to calculate the unidirectional fluxes, which correspond to the $^{86}Rb^+$ uptake, as described in [2, 4, 14]. In the Appendix we show expressions for the unidirectional fluxes.

Thermodynamic considerations place some restrictions on the parameter values. The principle of detailed balance [1] states that in the absence of an energetically driven process, the product of the rate constants encountered when traversing a cyclic reaction scheme in one direction must equal the corresponding product when traversing the scheme in the opposite direction. Applying this principle to the diagram in Figure 1, one gets from the inner cycle that

$$k_{\mathrm{be}} = \frac{k_{\mathrm{ff}} k_{\mathrm{fe}}}{k_{\mathrm{bf}}} \tag{2}$$

and from the outer cycle

$$k_{\mathrm{bf}}^{\mathrm{N}} = \frac{k_{\mathrm{ff}}^{\mathrm{N}} k_{\mathrm{fe}}}{k_{\mathrm{be}}}. \tag{3}$$

Similar constraints are obtained for the NKCC model when the principle is applied to Figure 2. It is important to point out that we obtained two equations for the thermodynamic constraint because there is competitive binding between K^+ and NH_4^+ when going from state E_0 to E_j ,

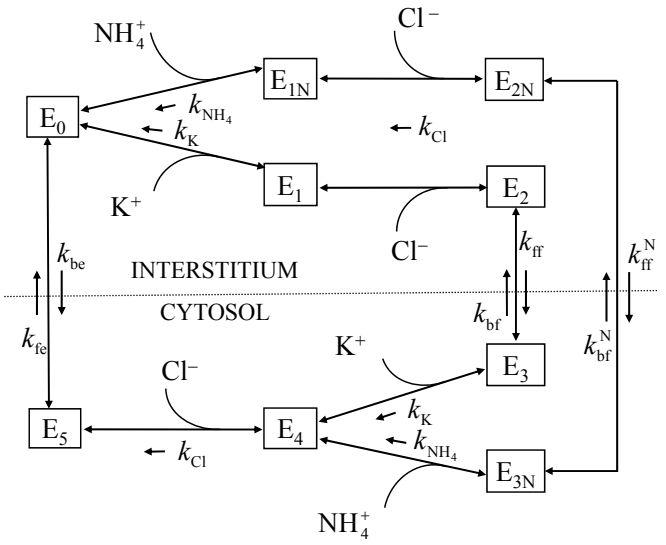

Figure 1: Kinetic diagram of the K-Cl cotransporter. k_{on} (not shown), on-binding rate constant (assumed equal for all reactions); k_j, off-binding rate constants (j =Cl, K, NH_4); k_{be}, k_{bf}, k_{fe}, k_{ff}, k_{bf}^{N}, k_{ff}^{N}, translocation rate constants; E_j, cotransporter fraction at state j ($j = 0, 1, \ldots, 5$ for the potassium cycle and $j = 0, 1\text{N}, 2\text{N}, 3\text{N}, 4, 5$ for the ammonium cycle).

$j = 1, 1N$ (or from E_4 to E_j , $j = 3, 3N$) in Figure 1 or from E_2 to E_j , $j = 3, 3N$ (or from E_8 to E_j , $j = 7, 7N$) in Figure 2. This means that for each cotransporter, once K^+ is bound, the cycle associated with NH_4^+ cannot be initiated and vice versa. In the model, we represent a population of cotransporters and E_j is the fraction of cotransporter in state j.

2.1 The direct method

For given parameter values, the direct method computes unidirectional fluxes for each ion involved in the model for various external concentrations of the corresponding ion over the range used in the experiments, whereas the external concentration values of the other ions are kept fixed. Then, for each concentration value of the varied ion, the unidirectional flux corresponding to the $^{86}Rb^+$ uptake is calculated from the cotransporter fraction values (which are computed using Equation (1)) by using Equations (46)–(49).

2.2 The optimization problem

A nonlinear least-squares problem was solved to estimate the unknown parameters, within prescribed ranges, by minimizing the differences between the model unidirectional fluxes, computed by means of the direct method, and the reported fluxes for the KCC1 and KCC4 for different Cl^-, K^+, and NH_4^+ concentrations [3, 15], or the reported fluxes for the NKCC2A, NKCC2B, and NKCC2F for different Na^+, Cl^-, K^+, and NH_4^+ concentrations [3, 17].

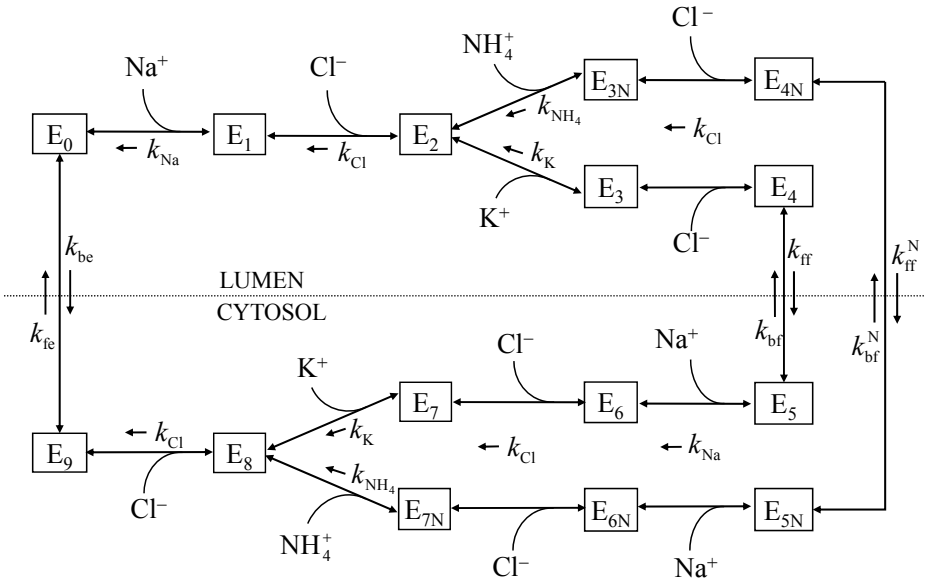

Figure 2: Kinetic diagram of the Na-K-2Cl cotransporter. k_{on} (not shown), on-binding rate constant (assumed equal for all reactions); k_j, off-binding rate constant (j =Na, Cl, K, NH_4); k_{be}, k_{bf}, k_{fe}, k_{ff}, k_{bf}^N, k_{ff}^N, translocation rate constants; E_j, cotransporter fraction at state j ($j = 0, 1, \ldots, 9$ for the potassium cycle and $j = 0, 1, 2, 3N, 4N, 5N, 6N, 7N, 8, 9$ for the ammonium cycle).

The optimization problem can be written as follows:

$$\min_{\mathbf{p}} \sum_{j=1}^{N} \left(J_{E,j} - J_{M,j}\left(\mathbf{p}\right)\right)^2, \tag{4}$$

$$\mathbf{p}_l \leq \mathbf{p} \leq \mathbf{p}_u, \tag{5}$$

where $\mathbf{J}_E$ and $\mathbf{J}_M$ are vectors containing the values of the experimental unidirectional fluxes and the unidirectional fluxes computed by the model, respectively, N is the number of data points of the ion flux curves, $\mathbf{p}$ is the vector of variable parameters, and $\mathbf{p}_l$ and $\mathbf{p}_u$ are the parameter lower and upper bounds, respectively. The inequality in (5) relating $\mathbf{p}_l$, $\mathbf{p}$, and $\mathbf{p}_u$ holds element by element. For both KCC1 and KCC4, N is equal to 23 data points for the flux curves of Cl^-, K^+ and NH_4^+. For NKCC2A, NKCC2B, and NKCC2F, N is equal to 33, 35, and 34 data points, respectively, corresponding to the flux curves of Na^+, Cl^-, K^+, and NH_4^+. The curves (three for the KCC and four for the NKCC) were fit simultaneously.

2.3 Experimental data

For use in the optimization procedure, it was necessary to normalize the data with respect to the maximum reaction rate constant V_{max}, because in [15, 17] the fluxes were expressed in nonstandard units of pmole/(oocyte hour). We obtained V_{max} estimates by fitting the Hill equation with specified Hill coefficients (1 for Na^+, K^+, and NH_4^+, 2 for Cl^-) to the data in each uptake curve using a nonlinear least-squares method. This fitting procedure provides an estimate of the apparent K_m; the values are listed in Table 4 for the KCC and in Table 6 for the NKCC for comparison with the values obtained with our cotransporter model using the parameter values

obtained with the optimization procedure wherein all the flux curves were fit simultaneously. The ammonium data of Bergeron et al. [3] was normalized with respect to the maximal experimental flux. Thus we computed $V_{\max}$ for these data values and renormalized them with respect to $V_{\max}$.
Parameter optimization algorithm (POA). With an initial value for the parameter vector $\mathbf{p}$ we computed an approximate solution for the optimization problem by using a trust-region method for nonlinear minimization with parameter bounds [6, 16]. To implement this method we used the MATLAB® function for large-scale optimization of nonlinear least-squares problems. This method is locally convergent and thus it calculates a local minimum. Hence, a parameter space exploration must be conducted to check for the possible occurrence of multiple optima or a global optimum, as described below.
Parameter exploration algorithm (PEA).

1. Generate a uniformly distributed population of M initial iterates for the optimization problem that are within the parameter ranges given on Table 2.
2. Starting with each initial iterate, execute independently the POA until convergence.
3. Select the optimum or optima showing the smallest optimization function value.

The value of M was set equal to 1,000, and we repeated the PEA three times starting with three different seeds to generate the pseudo-random number distribution (i.e., three realizations). The algorithms were implemented in MATLAB® (The MathWorks, Natick, MA) and executed in a computer with two Quad-Core Intel Xeon 2.26-GHz processors.

3 Results

The parameter values that were kept fixed during the optimization process are reported in Table 1. These are the on-binding rate constant k_{on}, the total amount of cotransporter E_{T}, and the intracellular concentrations for Na^+, Cl^-, K^+, and NH_4^+. Because, in the model equations, E_j represents the fraction of cotransporter in state j, the total amount of cotransporter is set equal to one. The assumed intracellular concentrations for Na^+, Cl^-, and K^+ are the same used before by us in the NKCC model [14] and are close to the values assumed by Weinstein [21]. Moreover, Weinstein [21] varied the intracellular concentrations of Na^+, Cl^-, and K^+ for an NKCC model and found small differences for the parameter values that fit the data. The parameter bounds $\mathbf{p}_{\text{l}}$ and $\mathbf{p}_{\text{u}}$ are reported in Table 2. The parameter bounds were selected to ensure that chemical reactions are faster than translocations and thus, for the optimum sets of parameters, ion-binding equilibrium holds.
For the KCC model, we used $^{86}Rb^+$ influx data as a function of the external Cl^-, K^+, and NH_4^+ concentrations for the KCC1 obtained from rabbit and for the KCC4 obtained from mouse [3, 15].

Table 1: Fixed parameter values

Parameter	Description	Value
k_{on}(l·mol^{-1}s^{-1})	on-binding rate constant	1.0×10^8
E_{T}(dimensionless)	total amount of cotransporter	1.0
C^{i}_{Na}(mM)	intracellular sodium concentration	7.0
C^{i}_{Cl} (mM)	intracellular chloride concentration	9.0
C^{i}_{K} (mM)	intracellular potassium concentration	124.0
$C^{\text{i}}_{\text{NH}_4}$ (mM)	intracellular ammonium concentration	2.0

Table 2: Variable parameter ranges

Parameter	Description	Range
k_{Na}, k_{Cl}, k_K and k_{NH_4} (s^{-1})	off-binding constants	$[10^5, 10^9]$
k_{fe}, k_{bf}, k_{ff}, and k_{bf}^N (s^{-1})	translocation rate constants	$[10^3, 10^5]$

The equilibrium constant $K_j = k_{on}/k_j$ ($l \cdot mol^{-1}$) ranges are $[10^{-1}, 10^3]$.

For the NKCC model, we used $^{86}Rb^+$ influx data as a function of the external Na^+, Cl^-, and K^+ concentrations for the NKCC2A, NKCC2B, and NKCC2F obtained from mouse [17], and as a function of the external NH_4^+ concentration for the NKCC2A obtained from rabbit [3]. To the best of our knowledge, measurements of NH_4^+ uptake by the NKCC2B and NKCC2F have not been made. In the absence of such data, we assumed in the optimization process that the NH_4^+ uptake for the B and F isoforms have the same K^+ affinity as the corresponding isoform.
We used the PEA to solve the optimization problem (4)–(5) to obtain parameters for the KCC and NKCC models, which are represented in Figures 1 and 2, as follows: to compute unidirectional fluxes as a function of the external Cl^- and K^+ concentrations in the KCC model, we used the inner cycle in Figure 1 by setting the NH_4^+ concentrations inside and outside the cell equal to zero and used the direct method to compute the fluxes. Then we computed the unidirectional flux as a function of the external NH_4^+ concentration by setting the K^+ concentrations inside and outside the cell equal to zero, this uses the outer cycle in Figure 1. Finally, the three curves are fit together by solving the optimization problem (4)–(5). For the NKCC model we proceeded in a similar manner. Figures 3 and 4 show the curves obtained for the optimal parameters of the KCC and NKCC models, respectively.
The optima and the coefficient of determination R^2 (6) for KCC1 and KCC4 are reported in Table 3 and for each variant of the NKCC2 isoform in Table 5.
The coefficient of determination is a good indicator of how well the model fits the data and it is computed as follows

$$R^2 = 1 - \frac{\sum_{j=1}^{N} \left(J_{E,j} - J_{M,j}\left(\mathbf{p}\right)\right)^2}{\sum_{j=1}^{N} \left(J_{E,j} - \overline{J}_E\right)^2}, \tag{6}$$

where $\mathbf{J}_E$ and $\mathbf{J}_M$ have the same meaning as in Equation (4) and $\overline{J}_E$ is the arithmetic mean of the elements of $\mathbf{J}_E$.
From Table 3, it is noteworthy that, for the KCC1 and KCC4 models, the values of R^2 are close to one, which means that the models fit the data quite well. However, the NKCC2B and NKCC2A models exhibit somewhat lower values of R^2 (see Table 5), which reflects slightly higher variability in the data for the NKCC2A and NKCC2B isoforms (see Figure 4A for the B isoform and Figure 4B for the A isoform).
Tables 4 and 6 list the half-maximum concentration (K_m) values for the optimum of each isoform for each cotransporter. The tables also report the experimental values obtained in [3, 15, 17] and the values that were recomputed by using least squares on the Hill equations (*vide supra*). Note that most of the model results are within or close to the experimental and recomputed ranges. There is a large difference in the K_m value of Cl^- for the KCC1 between the recomputed value and the published value by Mercado et al. [15], see Table 4. However, as one can see from Figure 6D in [15], using the reported value of V_{max} on page 30330 of [15], the value of K_m should be closer to 30 mM. For the NKCC, some of the recomputed K_m values differ slightly from the

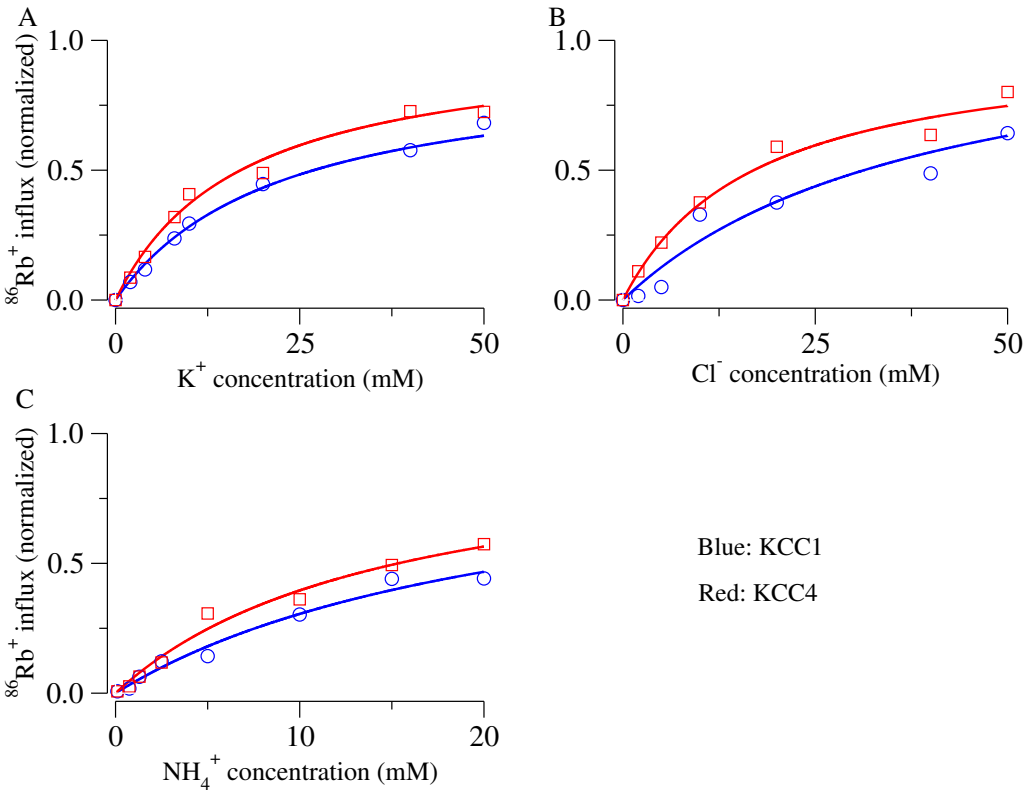

Figure 3: $^{86}Rb^+$ influx as a function of ion concentration for the KCC1 and KCC4 reported in [3, 15]. Plot (A): K^+ concentration was varied from 0 to 50 mM; Cl^- concentration was kept fixed to 50 mM. Plot (B): Cl^- concentration was varied from 0 to 50 mM; K^+ concentration was kept fixed to 50 mM. Plot (C): NH_4^+ concentration was varied from 0 to 20 mM; Cl^- concentration was fixed to 50 mM. Symbol represents experimental data; continuous line represents model result.

Table 3: Optimization results for the KCC models

Parameter	KCC1	KCC4
$K_{\mathrm{Cl}}(\mathrm{l{\cdot}mol^{-1}})$	46.190	998.36
$K_{\mathrm{K}}(\mathrm{l{\cdot}mol^{-1}})$	11.266	4.7534
$K_{\mathrm{NH_4}}(\mathrm{l{\cdot}mol^{-1}})$	6.4884	0.37984
$k_{\mathrm{ff}}(\mathrm{s^{-1}})$	1,000.4	2,224.1
$k_{\mathrm{bf}}(\mathrm{s^{-1}})$	2,832.4	1,001.3
$k_{\mathrm{fe}}(\mathrm{s^{-1}})$	1,018.6	4,867.4
$k_{\mathrm{be}}(\mathrm{s^{-1}})$	359.79	10,812.
$k_{\mathrm{ff}}^{\mathrm{N}}(\mathrm{s^{-1}})$	2,187.5	66,029.0
$k_{\mathrm{bf}}^{\mathrm{N}}(\mathrm{s^{-1}})$	6,193.1	29,726.0
R^2	0.97	0.98

R^2, coefficient of determination (6), is a good description of how well the model fits the data.

values published by Plata et al. [17], but this may only reflect differences in the methods used to estimate the value of K_{m}. Plata et al. [17] used linear regression of logarithm-transformed data

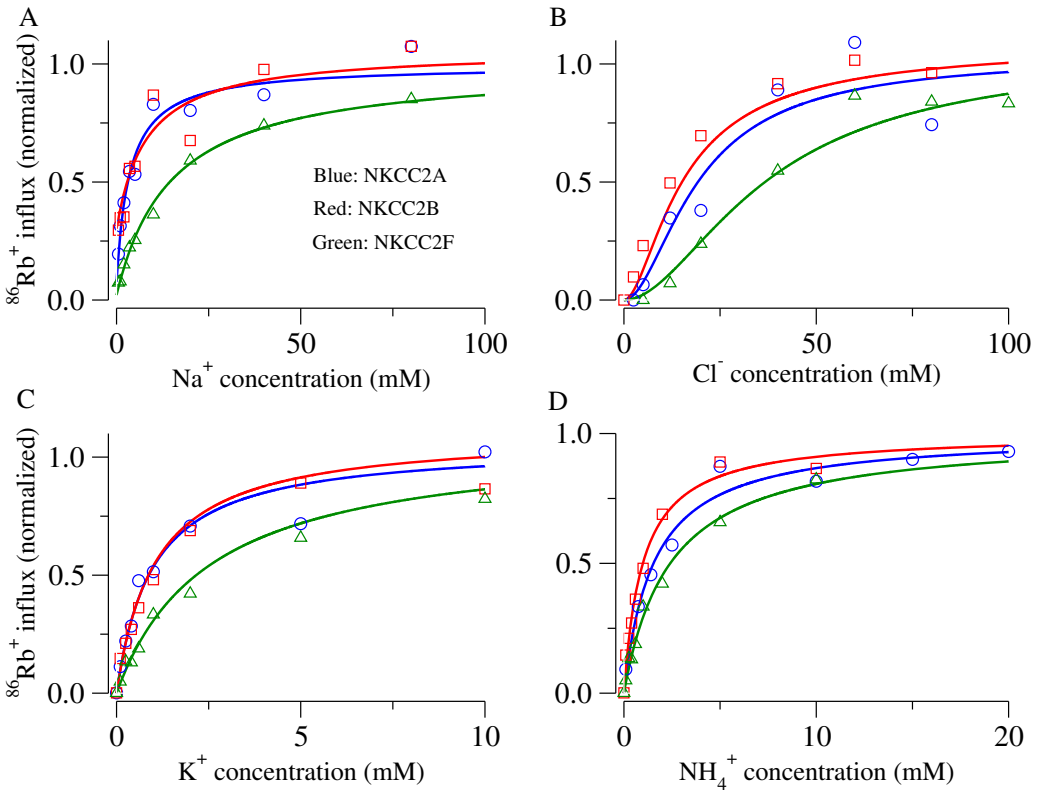

Figure 4: $^{86}Rb^+$ influx as a function of ion concentration for the NKCC2A, NKCC2B, and NKCC2F reported in [3, 17]. Plot (A): Na^+ concentration was varied from 0 to 100 mM; Cl^- and K^+ concentrations were kept fixed to 96 and 10 mM, respectively. Plot (B): Cl^- concentration was varied from 0 to 100 mM; Na^+ and K^+ concentrations were kept fixed to 96 and 10 mM, respectively. Plot (C): K^+ concentration was varied from 0 to 10 mM; Cl^- and Na^+ concentrations were both fixed to 96 mM. Plot (D): NH_4^+ concentration was varied from 0 to 20 mM; Cl^- and Na^+ concentrations were both fixed to 96 mM. Symbol represents experimental data; continuous line represents model result.

Table 4: Half-Maximum concentration (mM) for each ion for the KCC models

Ion species	Parameter Type	KCC1	KCC4
Cl^-	Model value	31.3	17.0
	Published value[1]	17.2±8.3	16.1±4.2
	Recomputed value	33.0±19.3	16.3±3.8
K^+	Model value	26.9	17.0
	Published value[1]	25.5±3.2	17.5 ±2.7
	Recomputed value	25.7±3.0	17.5±2.7
NH_4^+	Model value	22.8	15.3
	Published value[2]	22.9±13.5	13.5±5.5
	Recomputed value	22.8±9.3	15.4±4.8

[1]Mercado et al. [15]
[2]Bergeron et al. [3]

Table 5: Optimization results for the NKCC models

Parameter	NKCC2A	NKCC2B	NKCC2F
$K_{Na}(l{\cdot}mol^{-1})$	430.48	727.97	137.50
$K_{Cl}(l{\cdot}mol^{-1})$	136.99	1,000.0	750.99
K_K $(l{\cdot}mol^{-1})$	0.70907	0.13500	0.10000
$K_{NH_4}(l{\cdot}mol^{-1})$	2.6900	1.7488	1.3263
$k_{ff}(s^{-1})$	100,000.0	100,000.0	100,000.0
$k_{bf}(s^{-1})$	1,000.0	1,049.6	1,000.0
$k_{fe}(s^{-1})$	1,200.7	7,626.6	4,872.8
$k_{be}(s^{-1})$	120,067.0	726,620.0	487,278.0
$k_{ff}^N(s^{-1})$	14,069.0	3,729.0	4,177.4
$k_{bf}^N(s^{-1})$	140.69.0	39.140	41.774
R^2	0.94	0.96	0.98

normalized with respect to the flux at the highest ion concentration which was assumed to be a measure of V_{max}. If the plateau region of the curve is not well defined, this will lead to underestimation of the K_m value.
Previously, we reported [14] K_m values for Cl^- considerably higher than the values reported by Plata et al. [17]. The reason is that there is a discrepancy between the values of extracellular Cl^- concentrations used to assess the uptake curves reported in the caption of Figure 5 in [17] and the values shown in the graph on Figure 5A of [17]. As a result the uptake graph we used was shifted; to see this, compare the graph on Figure 4B with the graph on Figure 2B in [14]. For this work, we obtained the raw data from Dr. Gerardo Gamba.

Table 6: Half-maximum concentration (mM) for each ion for the NKCC models

Ion species	Parameter Type	NKCC2A	NKCC2B	NKCC2F
Na^+	Model value	3.06	2.88	14.4
	Published value[1]	5.0±3.9	3.0 ± 0.6	20.6 ±7.2
	Recomputed value	2.95±0.62	2.78 ±0.92	14.4± 1.6
Cl^-	Model value	19.3	15.1	36.7
	Published value[1]	22.2±4.8	11.6 ±0.7	29.2± 2.1
	Recomputed value	19.6±5.5	11.7±1.2	34.3 ±4.8
K^+	Model value	0.875	0.866	2.16
	Published value[1]	0.96±0.16	0.76± 0.07	1.54± 0.16
	Recomputed value	0.88±0.19	0.98 ±0.12	2.41±0.29
NH_4^+	Model value	1.54	0.982	2.41
	Published value[2]	1.7±0.5	No data available	No data available
	Recomputed value	1.58±0.29	——	——

[1]Plata et al. [17]
[2]Bergeron et al. [3]

The model K_m value of Cl^- for the NKCC2B is slightly higher than the experimental (see Table 6

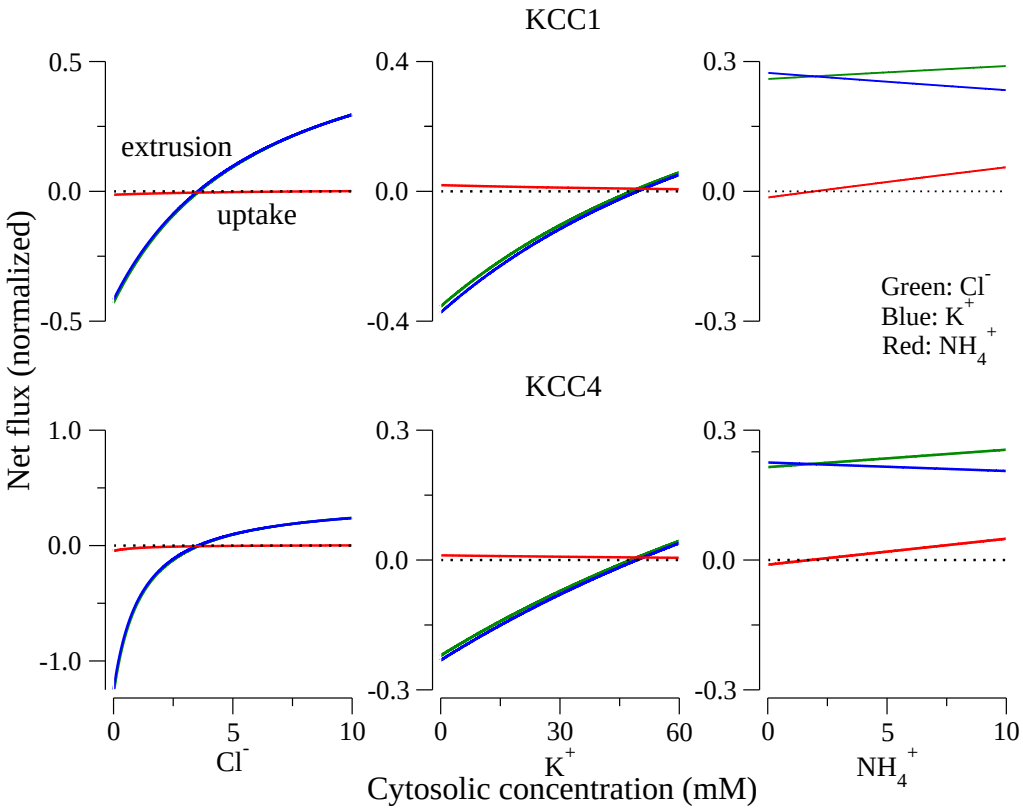

Figure 5: Net flux as a function of Cl^-, K^+, and NH_4^+ cytosolic concentrations for KCC1 and KCC4 in the cortex. Cytosolic concentrations of ions when kept fixed are: $[Cl^-]_i = 9$; $[K^+]_i = 124$; $[NH_4^+]_i = 2$. Interstitial concentrations are: $[Cl^-]_e = 110$; $[K^+]_e = 4$; $[NH_4^+]_e = 0.1$. Green, Cl^-; blue, K^+; red, NH_4^+.

and Figure 4B). However, this relatively "poor" fit compares with the fit obtained by others; for example, see Figure 3 in [21]. Recall that four curves are simultaneously fit, which may explain the differences between the model and experimental affinities for the NKCC2B. Nevertheless, the relationship between the location of the NKCC2 variants and the ion affinities holds:
NKCC2B K_m < NKCC2A K_m < NKCC2F K_m.
Figures 5–8 show the net fluxes computed with the optimal parameters for each ion for each cotransporter. We assumed a positive flux to be from the lumen to the interstitium. Thus, in the apical membrane, uptake is positive and extrusion is negative, whereas, in the basolateral membrane uptake is negative and extrusion is positive.
In Figure 5, we used low concentration values, as it is the case in the cortical TAL. We assumed that the concentrations of Cl^-, K^+, and NH_4^+ (except when varied) are, respectively, equal to 9, 124, and 2 mM in the cytosol and 110, 4, and 0.1 mM in the interstitium. In Figure 6, we used high concentration values, as it may be assumed in the medullary TAL. We chose the concentrations of Cl^-, K^+, and NH_4^+ (except when varied), respectively, equal to 35, 124, and 10 mM in the cytosol and 110, 5, and 2 mM in the interstitium.
From Figures 5 and 6, it is noteworthy that the interstitial ammonium concentration, which is higher in the medulla, makes a notable difference in the flux profiles. In the medulla (Figure 6), as the cytosolic ammonium is increased from zero, the uptake of ammonium decreases and when the cytosolic concentration of ammonium exceed 20 mM the cell extrudes it. Because the net flux of Cl^- is the sum of the net flux of K^+ and NH_4^+, the extrusion of K^+ is decreased. Further,

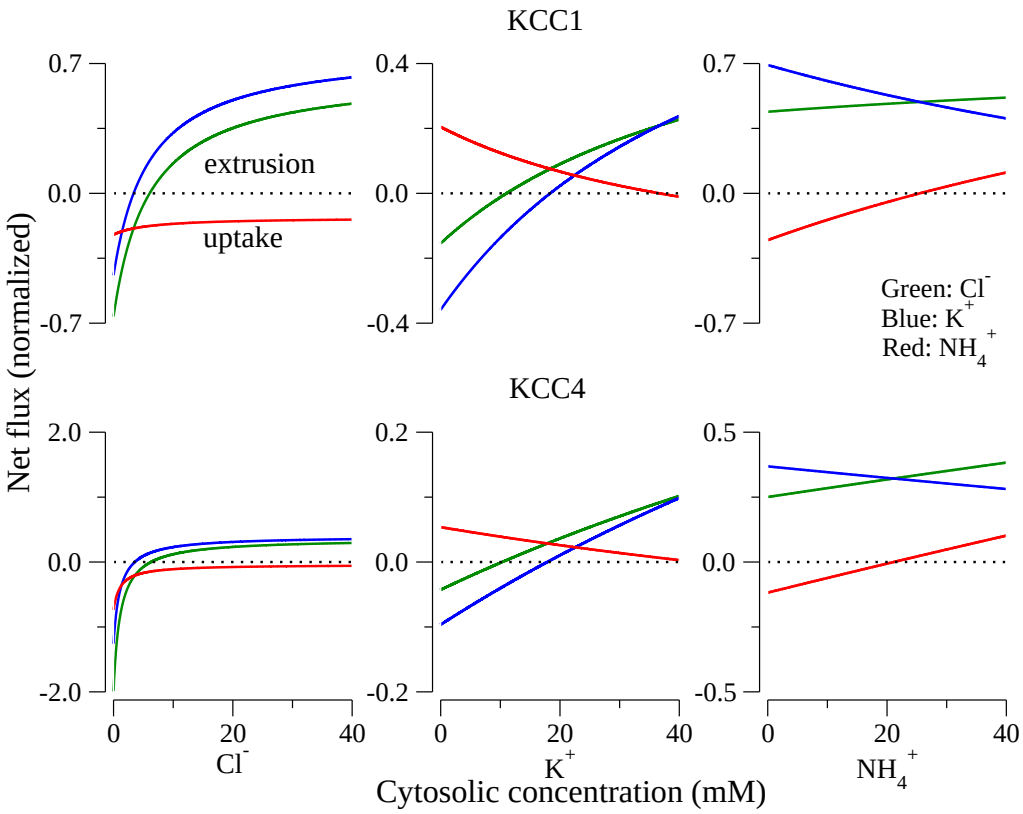

Figure 6: Net flux as a function of Cl^-, K^+, and NH_4^+ cytosolic concentrations for KCC1 and KCC4 in the outer medulla. Cytosolic concentrations of ions when kept fixed are: $[Cl^-]_i = 35$; $[K^+]_i = 124$; $[NH_4^+]_i = 10$. Interstitial concentrations are: $[Cl^-]_e = 110$; $[K^+]_e = 5$; $[NH_4^+]_e = 2$. Green, Cl^-; blue, K^+; red, NH_4^+.

Figure 6 illustrates the phenomenon of K^+/NH_4^+ exchange, which is predicted to occur at cytosolic concentrations where the chloride flux curve lies between the K^+ and NH_4^+ curves.
In Figure 7, we used low luminal concentration values, aiming to simulate the cortical TAL environment, and thus the concentrations of Na^+, Cl^-, K^+, and NH_4^+ (except when varied) were set, respectively, to 25, 30, 2, and 2 mM in the lumen and 7, 9, 124, and 2 in the cytosol. In Figure 8, we used high luminal concentrations, similar to those in the medullary TAL, and thus the Na^+, Cl^-, K^+, and NH_4^+ (except when varied) were set, respectively, to 150, 140, 10, and 20 mM in the lumen; in the cytosol we used the same concentrations as in the cortical case.
In Figure 7, at low luminal concentrations, as Na^+ and Cl^- are varied, Na^+, Cl^-, and K^+ net fluxes change from extrusion to uptake, whereas NH_4^+ is always taken up. These curves illustrate the augmentation of Na^+ uptake by luminal NH_4^+ (column D), and competition between K^+ and NH_4^+ (Columns C and D). The models also predict significant K^+/NH_4^+ exchange, which occurs when the Na^+ uptake curve lies between the K^+ and NH_4^+ curves. This phenomenon, which is most notable when luminal Na^+ and Cl^- concentrations are low, results in K^+ secretion into the lumen, an action that would tend to prevent luminal K^+ depletion.
In Figure 8, at high luminal ligand concentrations, the NKCC model quickly approach saturation as luminal Na^+ and Cl^- increases. Variation of luminal K^+ and NH_4^+ leads to only small increases of overall Na^+ transport, and there is significant competition between K^+ and NH_4^+. Note also that K^+/NH_4^+ exchange is only evident when luminal K^+ concentrations are low.

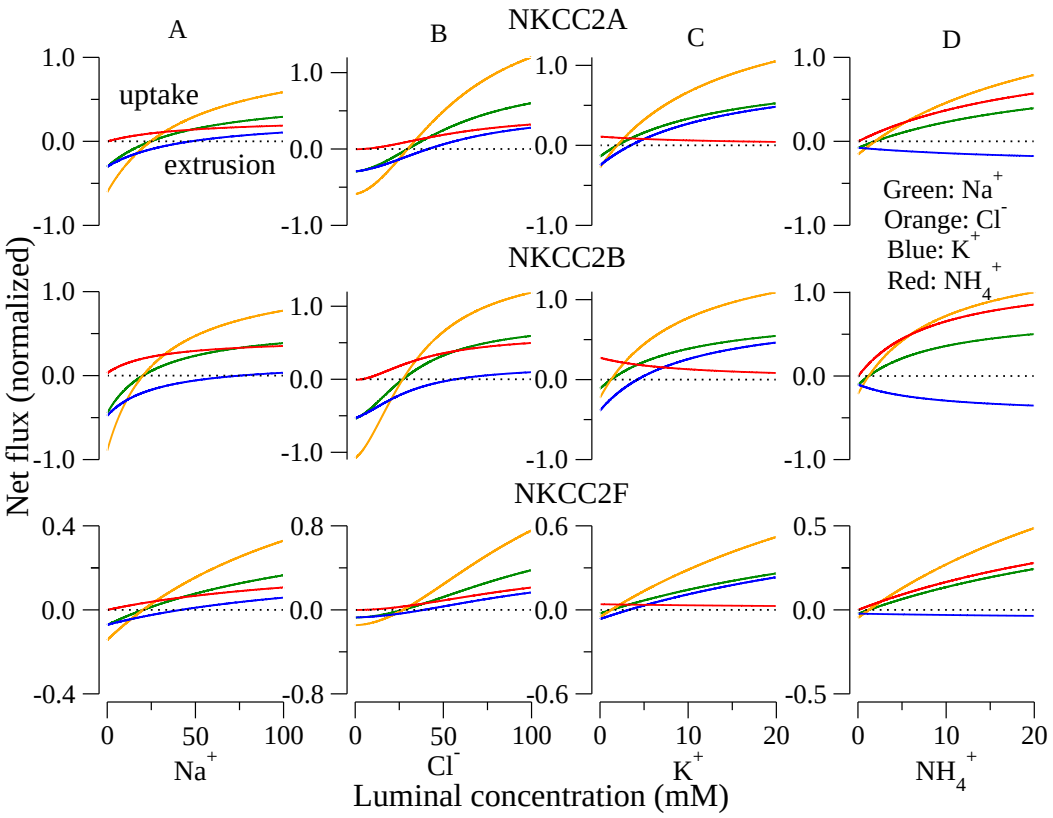

Figure 7: Net flux as a function of Na^+, Cl^-, K^+, and NH_4^+ luminal concentrations for NKCC2A, NKCC2B, and NKCC2F in the cortex. Luminal concentrations of ions when kept fixed are: $[Na^+]_e = 25$; $[Cl^-]_e = 30$; $[K^+]_e = 2$; $[NH_4^+]_e = 2$. Cytosolic concentrations of ions are: $[Na^+]_i = 7$; $[Cl^-]_i = 9$; $[K^+]_i = 124$; $[NH_4^+]_i = 2$. Green, Na^+; orange, Cl^-; blue, K^+; red, NH_4^+.

4 Discussion

In this work, we used an optimization algorithm with given sets of experimentally measured fluxes to compute parameter values for kinetic models of NKCC and KCC with transport of NH_4^+. Because different sets of parameters fit the experimental data with similar errors, we let the algorithm to systematically explore the parameter space by starting the optimization method with a large set of initial iterates uniformly distributed within the parameter space. We reported the solution that yields minimal error among the 1,000 solutions that were computed. Existence of multiple solutions has previously been observed in mathematical models of the NKCC [14, 21]. The resultant NKCC models showed ligand binding affinities in agreement with experimental findings, and at low luminal concentrations they exhibit substantial rates of K^+/NH_4^+ exchange (see Figure 7), whereas at high luminal concentrations the competition between K^+ and NH_4^+ was evident (see Figure 8).

Weinstein [21] formulated kinetic models for the KCC and NKCC with NH_4^+ transport. The models were posed in steady state and simplified by using the rapid-equilibrium assumption. As a result the fifteen equations in (16)–(30) reduce to two linear equations. Moreover, Weinstein argued that, in the simplified models, there are some parameters with free choice, which reduces the number of parameters that can be computed with these models.

In the present work, the kinetic models were posed as dynamical systems without assuming the

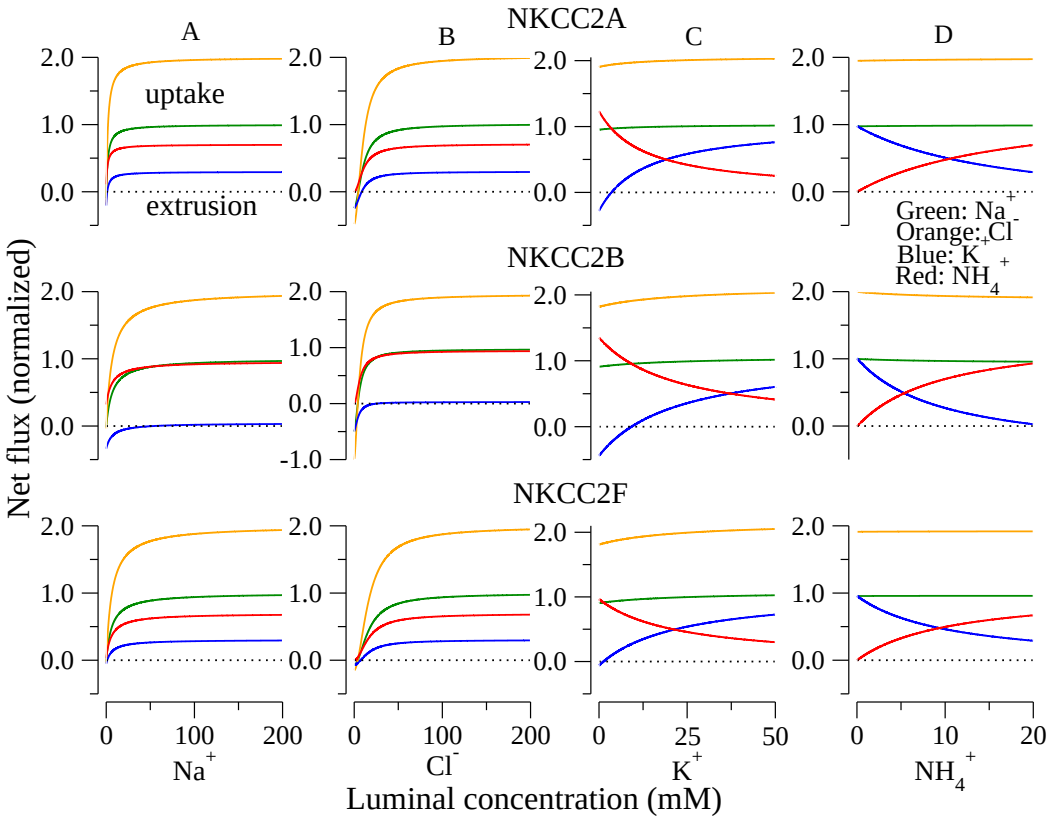

Figure 8: Net flux as a function of Na^+, Cl^-, K^+, and NH_4^+ luminal concentrations for NKCC2A, NKCC2B, and NKCC2F in the outer medulla. Luminal concentrations of ions when kept fixed are: $[Na^+]_e = 150$; $[Cl^-]_e = 140$; $[K^+]_e = 10$; $[NH_4^+]_e = 20$. Cytosolic concentrations of ions are: $[Na^+]_i = 7$; $[Cl^-]_i = 9$; $[K^+]_i = 124$; $[NH_4^+]_i = 2$. Green, Na^+; orange, Cl^-; blue, K^+; red, NH_4^+.

equilibrium binding approximation; the model Equations (7)–(15) and (16)–(30) were solved in steady state. Furthermore, the models used to compute the parameters are nonlinear. We used Equation (46) to fit the KCC data, (47) to fit the NH_4^+ transport by KCC, (48) to fit the NKCC data, and (49) to fit the NH_4^+ transport by NKCC. The expressions (46)–(49) are nonlinear with respect to the parameters and to compute E_0 in (46) and (47) the system of Equations (7)–(15) has to be solved in steady state (similarly, to compute E_2 in (48) and (49) the system of Equations (16)–(30) has to be solved), which increases the model nonlinearity. Owing to the nonlinearity of the models it is difficult, if not impossible, to determine the degrees of freedom of the parameters. For purpose of comparison, we report in Table 7 the parameters obtained by Weinstein [21] for the NKCC in the units we used. In Table 8 we report the values of K_m by using the parameters of Table 7 in our model; in parenthesis we show K_m values estimated from Figure 3 in [21] (Weinstein did not report these values). To find the K_m value from Figure 3 in [21], we assumed saturation at one and find the corresponding concentration value at 0.5. It is noteworthy that the Weinstein parameters decrease the binding affinities of our NKCC2 model; to see this, compare model values of K_m in Table 6 with the corresponding K_m values in Table 8. This is not surprising, because our NKCC2 model is much more nonlinear in the parameters than the reduced Weinstein model.

Finally, the data used to find the parameters related to the ammonium cycle in the NKCC transporter (outer cycle in Figures 2) came from a different laboratory using NKCC2 protein from

Table 7: Parameters reported by Weinstein [21] for the NKCC model

Parameter	NKCC2A	NKCC2B	NKCC2F
$K_{Na}(l{\cdot}mol^{-1})$	8.4175	3.6364	16.969
$K_{Cl}(l{\cdot}mol^{-1})$	11,320.0	12,259.0	76.220
K_K $(l{\cdot}mol^{-1})$	0.05345	0.1793	109.30
$K_{NH_4}(l{\cdot}mol^{-1})$	0.05345	0.1793	109.30
$k_{ff}(s^{-1})$	10,000.0	10,000.0	10,000.0
$k_{bf}(s^{-1})$	2,904.0	9,695.0	1,098.0
$k_{fe}(s^{-1})$	75,350.0	251,700.0	39,280.0
$k_{be}(s^{-1})$	259,470.0	259,618.0	357,741.0
$k_{ff}^N(s^{-1})$	2,000.0	2,000.0	2,000.0
$k_{bf}^N(s^{-1})$	580.80	1,939.0	219.60

Note that Weinstein reported the transporter binding affinity in units of M.

different species than the data used to identify the parameters of the potassium cycle (inner cycle in Figure 2). It would be desirable to have a full set of binding data all collected under the same conditions. In addition, it would be good to have measurements of obligate ion exchange (K^+/K^+ and Na^+/Na^+ exchange) and turnover rate, as this would provide additional insight into values of the translocation parameters.

These technical difficulties aside, the present study illustrates the fact that the KCC and NKCC transporters can exhibit a variety of behaviors depending on the concentrations of the ligands in the interstitium and tubular lumen. Of particular importance is K^+/NH_4^+ exchange by the NKCC transporter, which is predicted to occur when luminal Na^+ and Cl^- concentrations are low. Micropuncture samples collected near the macula densa in rats show that the early distal concentration of Na^+ is 20–25 mM and the K^+ concentration is ∼1–2 mM [18]. Potassium secretion by the NKCC2 transporter would supplement diffusive secretion through apical K^+ channels, and the stabilization of luminal K^+ levels would enhance Na^+ uptake. Further, the NH_4^+ entering the cell would, at least in part, be returned to the tubular lumen by the apical NHE transporter, which would result in the uptake of Na^+. Hence the cycling of NH_4^+ across the apical membrane of cortical TAL cells may enhance the cells ability to dilute the tubular fluid. Finally, Weinstein described the role of NH_4^+ on Na^+ uptake by the NKCC2 transporter as being catalytic. In the technical sense, this is incorrect, as a catalyst does not participate in the reaction, here ion uptake, that it accelerates. Rather, NH_4^+ is carried by the NKCC transporter, competes with K^+, can augment Na^+ uptake, and can be exchanged for K^+. None of these events is catalytic, but all deserve further study.

Table 8: Half-maximum concentration (mM) computed using Weinstein [21] parameters for the NKCC models

Ion species	NKCC2A	NKCC2B	NKCC2F
Na^+	9.13 (4.00)	7.35 (2.00)	20.1 (17.7)
Cl^-	29.6 (22.0)	22.0 (16.1)	42.3 (42.3)
K^+	1.56 (1.20)	0.803 (0.63)	1.98 (2.40)
NH_4^+	4.05	1.89	1.78

Values in parenthesis are estimated from Figure 3 in [21].

5 Appendix

5.1 Model Equations

Our KCC and NKCC models assume that the reaction cycles are in steady state and consist of linear systems of algebraic equations. The linear equations are obtained from more general systems of ordinary differential equations (ODE), which are shown below for both cotransporters with transport of NH_4^+.

KCC with NH_4^+. From Figure 1, the rate of change of each transporter state must be equal to the sum of all the reactions involving that state (conservation of cotransporter), which yield the following ODEs:

$$\frac{\mathrm{d}\,E_0}{\mathrm{d}\,t} = -k_{\mathrm{on}}C^{\mathrm{e}}_{\mathrm{K}}E_0 + k_{\mathrm{K}}E_1 - k_{\mathrm{be}}E_0 + k_{\mathrm{fe}}E_5 - k_{\mathrm{on}}C^{\mathrm{e}}_{\mathrm{NH_4}}E_0 + k_{\mathrm{NH_4}}E_{1\mathrm{N}}, \tag{7}$$

$$\frac{\mathrm{d}\,E_1}{\mathrm{d}\,t} = -k_{\mathrm{on}}C^{\mathrm{e}}_{\mathrm{Cl}}E_1 + k_{\mathrm{Cl}}E_2 - k_{\mathrm{K}}E_1 + k_{\mathrm{on}}C^{\mathrm{e}}_{\mathrm{K}}E_0, \tag{8}$$

$$\frac{\mathrm{d}\,E_{1\mathrm{N}}}{\mathrm{d}\,t} = -k_{\mathrm{on}}C^{\mathrm{e}}_{\mathrm{Cl}}E_{1\mathrm{N}} + k_{\mathrm{Cl}}E_{2\mathrm{N}} - k_{\mathrm{NH_4}}E_{1\mathrm{N}} + k_{\mathrm{on}}C^{\mathrm{e}}_{\mathrm{NH_4}}E_0, \tag{9}$$

$$\frac{\mathrm{d}\,E_2}{\mathrm{d}\,t} = -k_{\mathrm{ff}}E_2 + k_{\mathrm{bf}}E_3 - k_{\mathrm{Cl}}E_2 + k_{\mathrm{on}}C^{\mathrm{e}}_{\mathrm{Cl}}E_1, \tag{10}$$

$$\frac{\mathrm{d}\,E_{2\mathrm{N}}}{\mathrm{d}\,t} = -k^{\mathrm{N}}_{\mathrm{ff}}E_{2\mathrm{N}} + k^{\mathrm{N}}_{\mathrm{bf}}E_{3\mathrm{N}} - k_{\mathrm{Cl}}E_{2\mathrm{N}} + k_{\mathrm{on}}C^{\mathrm{e}}_{\mathrm{Cl}}E_{1\mathrm{N}}, \tag{11}$$

$$\frac{\mathrm{d}\,E_3}{\mathrm{d}\,t} = -k_{\mathrm{bf}}E_3 + k_{\mathrm{ff}}E_2 - k_{\mathrm{K}}E_3 + k_{\mathrm{on}}C^{\mathrm{i}}_{\mathrm{K}}E_4, \tag{12}$$

$$\frac{\mathrm{d}\,E_{3\mathrm{N}}}{\mathrm{d}\,t} = -k^{\mathrm{N}}_{\mathrm{bf}}E_{3\mathrm{N}} + k^{\mathrm{N}}_{\mathrm{ff}}E_{2\mathrm{N}} - k_{\mathrm{NH_4}}E_{3\mathrm{N}} + k_{\mathrm{on}}C^{\mathrm{i}}_{\mathrm{NH_4}}E_4, \tag{13}$$

$$\frac{\mathrm{d}\,E_4}{\mathrm{d}\,t} = -k_{\mathrm{Cl}}E_4 + k_{\mathrm{on}}C^{\mathrm{i}}_{\mathrm{Cl}}E_5 - k_{\mathrm{on}}C^{\mathrm{i}}_{\mathrm{K}}E_4 + k_{\mathrm{K}}E_3 - k_{\mathrm{on}}C^{\mathrm{i}}_{\mathrm{NH_4}}E_4 + k_{\mathrm{NH_4}}E_{3\mathrm{N}}, \tag{14}$$

$$\frac{\mathrm{d}\,E_5}{\mathrm{d}\,t} = -k_{\mathrm{on}}C^{\mathrm{i}}_{\mathrm{Cl}}E_5 + k_{\mathrm{Cl}}E_4 - k_{\mathrm{fe}}E_5 + k_{\mathrm{be}}E_0. \tag{15}$$

NKCC with NH_4^+. Similarly, from Figure 2, one gets the following system of equations for NKCC with NH_4^+

$$\frac{\mathrm{d}\,E_0}{\mathrm{d}\,t} = -k_{\mathrm{on}}C^{\mathrm{e}}_{\mathrm{Na}}E_0 + k_{\mathrm{Na}}E_1 - k_{\mathrm{be}}E_0 + k_{\mathrm{fe}}E_{9,} \tag{16}$$

$$\frac{\mathrm{d}\,E_1}{\mathrm{d}\,t} = -k_{\mathrm{on}}C^{\mathrm{e}}_{\mathrm{Cl}}E_1 + k_{\mathrm{Cl}}E_2 - k_{\mathrm{Na}}E_1 + k_{\mathrm{on}}C^{\mathrm{e}}_{\mathrm{Na}}E_{0,} \tag{17}$$

$$\frac{\mathrm{d}\,E_2}{\mathrm{d}\,t} = -k_{\mathrm{on}}C^{\mathrm{e}}_{\mathrm{K}}E_2 + k_{\mathrm{K}}E_3 - k_{\mathrm{Cl}}E_2 + k_{\mathrm{on}}C^{\mathrm{e}}_{\mathrm{Cl}}E_1 - k_{\mathrm{on}}C^{\mathrm{e}}_{\mathrm{NH_4}}E_2 + k_{\mathrm{NH_4}}E_{3\mathrm{N}}, \tag{18}$$

$$\frac{\mathrm{d}\,E_3}{\mathrm{d}\,t} = -k_{\mathrm{on}}C^{\mathrm{e}}_{\mathrm{Cl}}E_3 + k_{\mathrm{Cl}}E_4 - k_{\mathrm{K}}E_3 + k_{\mathrm{on}}C^{\mathrm{e}}_{\mathrm{K}}E_2, \tag{19}$$

$$\frac{\mathrm{d}\,E_{3\mathrm{N}}}{\mathrm{d}\,t} = -k_{\mathrm{on}}C^{\mathrm{e}}_{\mathrm{Cl}}E_{3\mathrm{N}} + k_{\mathrm{Cl}}E_{4\mathrm{N}} - k_{\mathrm{NH_4}}E_{3\mathrm{N}} + k_{\mathrm{on}}C^{\mathrm{e}}_{\mathrm{NH_4}}E_2, \tag{20}$$

$$\frac{\mathrm{d}\,E_4}{\mathrm{d}\,t} = -k_{\mathrm{ff}}E_4 + k_{\mathrm{bf}}E_5 - k_{\mathrm{Cl}}E_4 + k_{\mathrm{on}}C^{\mathrm{e}}_{\mathrm{Cl}}E_3, \tag{21}$$

$$\frac{\mathrm{d}\,E_{4\mathrm{N}}}{\mathrm{d}\,t} = -k^{\mathrm{N}}_{\mathrm{ff}}E_{4\mathrm{N}} + k^{\mathrm{N}}_{\mathrm{bf}}E_{5\mathrm{N}} - k_{\mathrm{Cl}}E_{4\mathrm{N}} + k_{\mathrm{on}}C^{\mathrm{e}}_{\mathrm{Cl}}E_{3\mathrm{N}}, \tag{22}$$

$$\frac{\mathrm{d}\,E_5}{\mathrm{d}\,t} = -k_{\mathrm{bf}}E_5 + k_{\mathrm{ff}}E_4 - k_{\mathrm{Na}}E_5 + k_{\mathrm{on}}C^{\mathrm{i}}_{\mathrm{Na}}E_6, \tag{23}$$

$$\frac{\mathrm{d}\,E_{5\mathrm{N}}}{\mathrm{d}\,t} = -k^{\mathrm{N}}_{\mathrm{bf}}E_{5\mathrm{N}} + k^{\mathrm{N}}_{\mathrm{ff}}E_{4\mathrm{N}} - k_{\mathrm{Na}}E_{5\mathrm{N}} + k_{\mathrm{on}}C^{\mathrm{i}}_{\mathrm{Na}}E_{6\mathrm{N}}, \tag{24}$$

$$\frac{\mathrm{d}\,E_6}{\mathrm{d}\,t} = -k_{\mathrm{on}}C^{\mathrm{i}}_{\mathrm{Na}}E_6 + k_{\mathrm{Na}}E_5 - k_{\mathrm{Cl}}E_6 + k_{\mathrm{on}}C^{\mathrm{i}}_{\mathrm{Cl}}E_7, \tag{25}$$

$$\frac{\mathrm{d}\,E_{6\mathrm{N}}}{\mathrm{d}\,t} = -k_{\mathrm{on}}C^{\mathrm{i}}_{\mathrm{Na}}E_{6\mathrm{N}} + k_{\mathrm{Na}}E_{5\mathrm{N}} - k_{\mathrm{Cl}}E_{6\mathrm{N}} + k_{\mathrm{on}}C^{\mathrm{i}}_{\mathrm{Cl}}E_{7\mathrm{N}}, \tag{26}$$

$$\frac{\mathrm{d}\,E_7}{\mathrm{d}\,t} = -k_{\mathrm{on}}C^{\mathrm{i}}_{\mathrm{Cl}}E_7 + k_{\mathrm{Cl}}E_6 - k_{\mathrm{K}}E_7 + k_{\mathrm{on}}C^{\mathrm{i}}_{\mathrm{K}}E_8, \tag{27}$$

$$\frac{\mathrm{d}\,E_{7\mathrm{N}}}{\mathrm{d}\,t} = -k_{\mathrm{on}}C^{\mathrm{i}}_{\mathrm{Cl}}E_{7\mathrm{N}} + k_{\mathrm{Cl}}E_{6\mathrm{N}} - k_{\mathrm{NH_4}}E_{7\mathrm{N}} + k_{\mathrm{on}}C^{\mathrm{i}}_{\mathrm{NH_4}}E_8, \tag{28}$$

$$\frac{\mathrm{d}\,E_8}{\mathrm{d}\,t} = -k_{\mathrm{on}}C^{\mathrm{i}}_{\mathrm{K}}E_8 + k_{\mathrm{K}}E_7 - k_{\mathrm{Cl}}E_8 + k_{\mathrm{on}}C^{\mathrm{i}}_{\mathrm{Cl}}E_9 - k_{\mathrm{on}}C^{\mathrm{i}}_{\mathrm{NH_4}}E_8 + k_{\mathrm{NH_4}}E_{7\mathrm{N}}, \tag{29}$$

$$\frac{\mathrm{d}\,E_9}{\mathrm{d}\,t} = -k_{\mathrm{on}}C^{\mathrm{i}}_{\mathrm{Cl}}E_9 + k_{\mathrm{Cl}}E_8 - k_{\mathrm{fe}}E_9 + k_{\mathrm{be}}E_0, \tag{30}$$

where C^l_j is the solute concentration of ion j in the intracellular ($l = \mathrm{i}$) or extracellular ($l = \mathrm{e}$) space; $E_j = E_j(t)$ is the fraction of cotransporter in state j; k_j is the release rate constant ($j = \mathrm{Na}$, Cl, K, $\mathrm{NH_4}$); k_{on} is the binding rate constant, assumed equal for all ionic bindings; ion binding and release rate constants are assumed the same on either side of the membrane; k_{ff}, k_{bf}, $k^{\mathrm{N}}_{\mathrm{ff}}$, and $k^{\mathrm{N}}_{\mathrm{bf}}$ are the forward and backward translocation rate constants for loaded transporter; k_{fe} and k_{be} are the forward and backward translocation rate constants for empty transporter. Adding Equations (7)–(15) and noting that the derivative of the sum of the $E_j(t)$s is equal to zero, implies Equation (31), where E_{T} is a constant

$$E_{\mathrm{T}} = \sum_{j=0}^{5} E_j(t) + \sum_{j=1}^{3} E_{j\mathrm{N}}(t) \tag{31}$$

Moreover, from Equation (31) one obtains

$$E_5(t) = E_{\mathrm{T}} - \sum_{j=0}^{4} E_j(t) - \sum_{j=1}^{3} E_{j\mathrm{N}}(t), \tag{32}$$

which makes Equation (15) redundant. By replacing E_5 in Equations (7)–(14) by the expression in Equation (32), the ODE system for the KCC model with NH_4^+ reduces to a system of eight equations in eight unknowns. At steady state, all of the derivatives in Equations (7)–(14) are zero, and the model reduces to a system of linear equations.

Proceeding in a similar way for the NKCC with NH_4^+, one gets

$$E_9(t) = E_{\mathrm{T}} - \sum_{j=0}^{8} E_j(t) - \sum_{j=3}^{7} E_{j\mathrm{N}}(t). \tag{33}$$

Now Equation (30) is redundant and by replacing E_9 in Equations (16)–(29) by the expression in Equation (33), the ODE system reduces to a system of fourteen equations in fourteen unknowns. At steady state the model reduces to a system of linear equations.

5.2 $^{86}Rb^+$ unidirectional influx

Our approach follows the unidirectional flux treatment of Britton [4] and Benjamin and Johnson[2]. The unidirectional influx of $^{86}Rb^+$ corresponds to the unidirectional transport between the transporter states where K^+ (or NH_4^+) is bound outside the cell and the state where it is released inside the cell. For KCC with NH_4^+ the unidirectional influx is the transport from E_0 to E_4 through the inner cycle for K^+ and through the outer cycle for NH_4^+ (Figure 1). For the NKCC with NH_4^+ the unidirectional influx is the transport from E_2 to E_8 through the inner cycle for K^+ and through the outer cycle for NH_4^+ (Figure 2).
The forward and backward unidirectional fluxes for two consecutive states (i and j) outside the cell are as follows:

$$J_{ij} = k_{\mathrm{on}} C_s^{\mathrm{e}} E_i \tag{34}$$

and

$$J_{ji} = k_s E_j, \tag{35}$$

where $C_s^{\mathrm{e}}$and k_s are, respectively, the external concentrations and the off-binding rate constants of the ions involved in the reaction. Inside the cell the forward and backward unidirectional fluxes of two consecutive states are

$$J_{ij} = k_s E_i \tag{36}$$

and

$$J_{ji} = k_{\mathrm{on}} C_s^{\mathrm{i}} E_j. \tag{37}$$

Now, consider three consecutive reactions, e.g., from the cotransporter fraction in state 0 to the fraction in state 2 in Figure 1. The unidirectional flux from state 0 to state 2 (J_{02}) is equal to the flux from state 0 to state 1 (J_{01}) multiplied by the probability that state 1 proceeds to state 2 instead of returning to state 0 $\left(\frac{J_{12}}{J_{12}+J_{10}}\right)$, i.e.,

$$J_{02} = \frac{J_{01} J_{12}}{J_{12} + J_{10}}. \tag{38}$$

Similarly, the unidirectional flux from state 2 to state 0 is given by

$$J_{20} = \frac{J_{10} J_{21}}{J_{12} + J_{10}}. \tag{39}$$

In general, the unidirectional fluxes from state i to state j, $j = i+2, i+3, \ldots$ are computed by using the following recursive formulas

$$J_{ij} = \frac{J_{i,j-1} J_{j-1,j}}{J_{j-1,j} + J_{j-1,i}} \tag{40}$$

and

$$J_{ji} = \frac{J_{j-1,i} J_{i,j-1}}{J_{j-1,j} + J_{j-1,i}}. \tag{41}$$

The unidirectional fluxes corresponding to the $^{86}Rb^+$ uptake for the KCC (Figure 1) are

$$J_{04} = \frac{J_{03} J_{34}}{J_{34} + J_{30}} \tag{42}$$

for the inner cycle, and

$$J_{04}^{\mathrm{N}} = \frac{J_{03}^{\mathrm{N}} J_{34}^{\mathrm{N}}}{J_{34}^{\mathrm{N}} + J_{30}^{\mathrm{N}}} \tag{43}$$

for the outer cycle. For the NKCC (Figure 2) the unidirectional fluxes are

$$J_{28} = \frac{J_{27} J_{78}}{J_{78} + J_{72}} \tag{44}$$

for the inner cycle, and

$$J_{28}^{\mathrm{N}} = \frac{J_{27}^{\mathrm{N}} J_{78}^{\mathrm{N}}}{J_{78}^{\mathrm{N}} + J_{72}^{\mathrm{N}}} \tag{45}$$

for the outer cycle.
By substituting in the recursive formula one can get explicit formulas for Equations (42)–(45)

$$J_{04} = \frac{k_{\mathrm{on}}^2 k_{\mathrm{ff}} C_{\mathrm{K}}^{\mathrm{e}} C_{\mathrm{Cl}}^{\mathrm{e}} E_0}{k_{\mathrm{Cl}} k_{\mathrm{K}} + k_{\mathrm{ff}} k_{\mathrm{K}} + k_{\mathrm{ff}} k_{\mathrm{on}} C_{\mathrm{Cl}}^{\mathrm{e}} + k_{\mathrm{Cl}} k_{\mathrm{bf}}}, \tag{46}$$

$$J_{04}^{\mathrm{N}} = \frac{k_{\mathrm{on}}^2 k_{\mathrm{ff}}^{\mathrm{N}} C_{\mathrm{NH_4}}^{\mathrm{e}} C_{\mathrm{Cl}}^{\mathrm{e}} E_0}{k_{\mathrm{Cl}} k_{\mathrm{NH_4}} + k_{\mathrm{ff}}^{\mathrm{N}} k_{\mathrm{NH_4}} + k_{\mathrm{ff}}^{\mathrm{N}} k_{\mathrm{on}} C_{\mathrm{Cl}}^{\mathrm{e}} + k_{\mathrm{Cl}} k_{\mathrm{bf}}^{\mathrm{N}}}, \tag{47}$$

$$J_{28} = \frac{k_{\mathrm{on}}^2 k_{\mathrm{ff}} k_{\mathrm{Na}} k_{\mathrm{Cl}} C_{\mathrm{K}}^{\mathrm{e}} C_{\mathrm{Cl}}^{\mathrm{e}} E_2}{D_1}, \tag{48}$$

and

$$J_{28}^{\mathrm{N}} = \frac{k_{\mathrm{on}}^2 k_{\mathrm{ff}}^{\mathrm{N}} k_{\mathrm{Na}} k_{\mathrm{Cl}} C_{\mathrm{NH_4}}^{\mathrm{e}} C_{\mathrm{Cl}}^{\mathrm{e}} E_2}{D_2}, \tag{49}$$

where

$$\begin{aligned} D_1 \;=\; & k_{\mathrm{on}} k_{\mathrm{ff}} k_{\mathrm{Na}} k_{\mathrm{Cl}} C_{\mathrm{Cl}}^{\mathrm{e}} + k_{\mathrm{ff}} k_{\mathrm{Na}} k_{\mathrm{Cl}} k_{\mathrm{K}} + k_{\mathrm{Na}} k_{\mathrm{Cl}}^2 k_{\mathrm{K}} + k_{\mathrm{bf}} k_{\mathrm{Cl}}^2 k_{\mathrm{K}} + k_{\mathrm{on}} k_{\mathrm{bf}} k_{\mathrm{K}} k_{\mathrm{Cl}} C_{\mathrm{Na}}^{\mathrm{i}} \\ & + k_{\mathrm{on}}^2 k_{\mathrm{bf}} k_{\mathrm{Cl}} C_{\mathrm{Na}}^{\mathrm{i}} C_{\mathrm{Cl}}^{\mathrm{i}} \end{aligned}$$

and

$$\begin{aligned} D_2 \;=\; & k_{\mathrm{on}} k_{\mathrm{ff}}^{\mathrm{N}} k_{\mathrm{Na}} k_{\mathrm{Cl}} C_{\mathrm{Cl}}^{\mathrm{e}} + k_{\mathrm{ff}}^{\mathrm{N}} k_{\mathrm{Na}} k_{\mathrm{Cl}} k_{\mathrm{NH_4}} + k_{\mathrm{Na}} k_{\mathrm{Cl}}^2 k_{\mathrm{NH_4}} + k_{\mathrm{bf}}^{\mathrm{N}} k_{\mathrm{Cl}}^2 k_{\mathrm{NH_4}} + k_{\mathrm{on}} k_{\mathrm{bf}}^{\mathrm{N}} k_{\mathrm{NH_4}} k_{\mathrm{Cl}} C_{\mathrm{Na}}^{\mathrm{i}} \\ & + k_{\mathrm{on}}^2 k_{\mathrm{bf}}^{\mathrm{N}} k_{\mathrm{Cl}} C_{\mathrm{Na}}^{\mathrm{i}} C_{\mathrm{Cl}}^{\mathrm{i}}. \end{aligned}$$

Note that the unidirectional fluxes are function of the binding rates, the translocation rates, the ion concentrations, and only of the transporter state where the tracer initially is bound, E_0 for KCC and E_2 for NKCC.
Each entry of the vector of the model unidirectional fluxes, $\mathbf{J}_M(\mathbf{p})$ in Equation (4), consists of the value of J_{04} for the KCC or J_{28} for the NKCC for each ion at each concentration value. Here $\mathbf{p}$ is

the vector of variable parameters.

Acknowledgments

We would like to thank Dr. Gerardo Gamba for kindly providing us the raw data of the oocyte experiments for the NKCC2. Portions of this work were presented in poster form at The Experimental Biology Meeting 2007 (Kinetic Models for Ammonium Transport by the NKCC2 Cotransporter, *FASEB J.* 21: 736.7) and The Experimental Biology Meeting 2009 (Parameter Estimation for Models of NH_4^+ Transport by the Renal Na-K-2Cl Cotransporter, *FASEB J.* 23: 602.22).

Grants

This research was supported in part by the National Institutes of Health grant SC1GM084744 from the National Institute of General Medical Sciences and a subcontract to grant DK-042091.

References

[1] RA Alberty. Principle of detailed balance in kinetics. *A J Chem Educ*, 81:1206–1209, 2004.

[2] BA Benjamin and EA Johnson. A quantitative description of the Na-K-2Cl cotransporter and its conformity to experimental data. *Am J Physiol*, 273:F473–482, 1997.

[3] MJ Bergeron, E Gagnon, B Wallendorff, JY Lapointe, and P Isenring. Ammonium transport and pH regulation by K^+-Cl^- cotransporters. *Am J Physiol Renal Physiol*, 285:F68–78, 2003.

[4] HG Britton. The concept and use of flux measurements in enzyme studies. A theoretical analysis. *Arch Biochem Biophysic*, 117:167–183, 1966.

[5] H Chang and T Fujita. A kinetic model of the thiazide-sensitive Na-Cl cotransporter. *Am J Physiol*, 276:F952–959, 1999.

[6] TF Coleman and Y Li. An interior, trust region approach for nonlinear minimization subject to bounds. *SIAM J Optimiz*, 6:418–445, 1996.

[7] E Gagnon, MJ Bergeron, GM Brunet, ND Daigle, CF Simard, and P Isenring. Molecular mechanisms of Cl^- transport by the renal Na^+-K^+-Cl^- cotransporter: Identification of an intracellular locus that may form part of a high affinity Cl^--binding site. *J Biol Chem*, 279:5648–5654, 2004.

[8] E Gagnon, MJ Bergeron, ND Daigle, MH Lefoll, and P Isenring. Molecular mechanisms of cation transport by the renal Na^+-K^+-Cl^- cotransporter: Structural insight into the operating characteristics of the ion transport sites. *J Biol Chem*, 280:32555–32563, 2005.

[9] DW Good. Ammonium transport by the thick ascending limb of Henle's loop. *Annu Rev Physiol*, 56:623–647, 1994.

[10] M Haas and B Forbush III. The Na-K-Cl cotransporter of secretory epithelia. *Annu Rev Physiol*, 62:515–534, 2000.

[11] R Kinne, E Kinne-Saffran, H Schutz, and B Scholermann. Ammonium transport in medullary thick ascending limb of rabbit kidney: Involvement of the Na^+,K^+,Cl^--cotransporter. *J Membrane Biol*, 94:279–284, 1986.

[12] C Lytle and TJ McManus. A minimal kinetic model of (Na-K-Cl) cotransport with ordered binding and glide symmetry. *J Gen Physiol*, 88:36a, 1986.

[13] C Lytle, TJ McManus, and Haas M. A model of Na-K-2Cl cotransport based on ordered ion binding and glide symmetry. *Am J Physiol*, 274:C299–309, 1998.

[14] M Marcano, HM Yang, A Nieves-González, C Clausen, and LC Moore. Parameter estimation for mathematical models of NKCC2 cotransporter isoforms. *Am J Physiol Renal Physiol*, 296:F369–381, 2009.

[15] A Mercado, L Song, N Vázquez, DB Mount, and G Gamba. Functional comparison of the K^+-Cl^- cotransporters KCC1 and KCC4. *J Biol Chem*, 275:30326–30334, 2000.

[16] JJ Moré and DC Sorensen. Computing a trust region step. *SIAM J Sci Stat Comp*, 3:553–572, 1983.

[17] C Plata, P Meade, N Vázquez, SC Hebert, and G Gamba. Functional properties of the apical Na^+-K^+-$2Cl^-$ cotransporter isoforms. *J Biol Chem*, 277:11004–11012, 2002.

[18] V Vallon, H Osswald, R Blantz, and S Thomson. Potential role of luminal potassium in tubuloglomerular feedback. *J Am Soc Nephrol*, 8:1831–1837, 1997.

[19] KE van Holde. A hypothesis concerning diffusion-limited protein-ligand interactions. *Biophys Chem*, 101-102:249–254, 2002.

[20] ID Weiner and LL Hamm. Molecular mechanisms of renal ammonia transport. *Annu Rev Physiol*, 69:317–340, 2007.

[21] AM Weinstein. A mathematical model of rat ascending Henle limb. I. Cotransporter function. *Am J Physiol Renal Physiol*, 298:F512–F524, 2010.